Tuning Thermal Transport in Chain-Oriented Conducting Polymers for Enhanced Thermoelectric Efficiency: A Computational Study

*Wen Shi, Zhigang Shuai, and Dong Wang**

Thermoelectric polymers should be electron-crystal and phonon-glass to efficiently interconvert heat and electricity. Herein, by using molecular dynamics simulations, it is demonstrated that engineering phonon transport in conducting polymers by tailoring its degree of polymerization can effectively improve the energy conversion efficiency. This is based on the separated length scales that charge carriers and phonons travel along the polymer backbone. By tuning the chain length and the crystallinity of chain-oriented poly(3,4-ethylenedioxythiophene) fibers, a dramatic decrease of the axial thermal conductivity to 0.97 W m^{-1} K^{-1} has been observed in rationally designed polymer fibers with the crystallinity of 0.49 and the relative molecular weight of 5600. The dimensionless thermoelectric figure of merit at 298 K has been enhanced to 0.48, which is approximately one order of magnitude higher than that in crystalline polymers.

1. Introduction

Thermal conductivity is a pivotal property of polymers, which significantly impacts the product reliability and device performance. Lately, conducting polymers as promising candidate thermoelectric (TE) materials to interconvert heat and electricity have attracted intense interest.[1] In TE applications poor heat conduction often results in efficient energy conversion. The efficiency of a TE material is quantified by a physical parameter known as the dimensionless figure of merit $zT = S^2\sigma T/\kappa$.[2] In solid materials, both charge carriers and lattice vibrations conduct heat. To achieve a high TE efficiency, excellent electrical transport properties and poor thermal transport properties should simultaneously exist in TE materials, which is known as the electron-crystal and phonon-glass criteria.[3] For conventional inorganic TE materials, electronic band engineering and phonon engineering have been demonstrated as two effective strategies to improve the TE efficiency, and these strategies are often combined to achieve the best TE performance.[4] The efficient TE materials are usually semiconductors, with high electrical conductivity, decent Seebeck coefficient, and low thermal conductivity.

For polymeric TE materials, efforts have been made to optimize charge transport properties by engineered chemical or electrochemical doping.[5] For example, by reducing the dopant volume in poly(3,4-ethylenedioxythiophene) (PEDOT) doped by poly(styrenesulphonate) (PSS), a high zT value of 0.42 is achieved,[6] which has successfully improved the zT value by two orders of magnitude.[7] Through the accurate control of carrier concentration in PEDOT doped by p-toluenesulfonate (Tos), a zT of 0.25[8] and a record large power factor (PF = $S^2\sigma$) of 1270 μW m^{-1} K^{-2}[9] are realized. Our previous theoretical investigation of doping effects on TE properties of "ideal" crystalline lightly doped PEDOT:Tos unraveled that by tuning the doping level a power factor of 3150 μW m^{-1} K^{-2} along the polymer chain and 209 μW m^{-1} K^{-2} in the π–π stacking direction can be realized.[10] However, engineered thermal transport in conducting polymers for enhanced TE efficiency has never been reported.

Polymers are amorphous by nature and often featured with low thermal conductivity and low carrier mobility. High mobility in D–A polymers has been reported and it has been ascribed to the increased chain alignment of these polymers.[11] It is also recognized that increased structural order and molecular organization in PEDOT lead to simultaneous increase of Seebeck coefficient and electrical conductivity, which gives rise to a large TE power factor.[12] Nevertheless, polymeric materials with ordered structures have been found to exhibit incredibly high lattice thermal conductivity, which is undoubtedly adverse to the acquisition of high zT (**Figure 1**a). Such as in high-quality ultradrawn polyethylene (PE) single crystalline nanofibers, the lattice thermal conductivity reaches 104 W m^{-1} K^{-1}, which is even higher than plenty of pure metals.[13] For the above reasons, both increased chain alignment and some extents of

Dr. W. Shi, Prof. Z. G. Shuai, Prof. D. Wang
MOE Key Laboratory of Organic OptoElectronics and Molecular Engineering
Department of Chemistry
Tsinghua University
Beijing 100084, P. R. China
E-mail: dong913@tsinghua.edu.cn

Prof. Z. G. Shuai
Key Laboratory of Organic Solids
Beijing National Laboratory for Molecular Science (BNLMS)
Institute of Chemistry
Chinese Academy of Sciences
Beijing 100190, P. R. China

Prof. Z. G. Shuai
Collaborative Innovation Center of Chemistry for Energy Materials
Xiamen University
Xiamen 351005, P. R. China

DOI: 10.1002/adfm.201702847

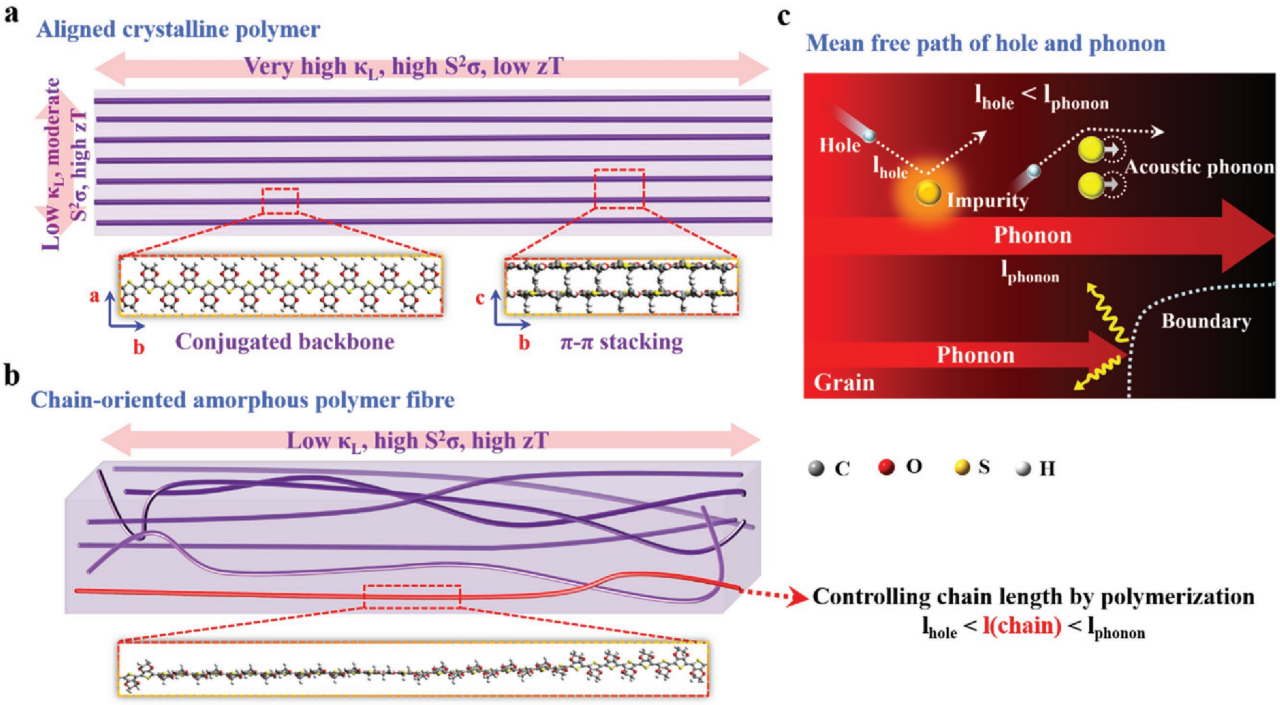

Figure 1. Schematic illustration of thermal and electrical transport in crystalline polymers and chain-oriented polymeric fibers. a) Anisotropic thermoelectric transport properties of crystalline polymers in the conjugated backbone and π–π stacking directions, respectively. The chemical structures of PEDOT are also displayed. b) Suppression of phonon transport in chain-oriented amorphous polymer fibers. The polymer chains extend along the long axial direction of the fiber. The polymer chains are tailored to be shorter than the mean free path of phonons while longer than that of charge carriers by controlling the degree of polymerization. c) Separated length scales of thermal and charge transport in the same crystallite. In general, the mean free path of phonons is much longer than that of charge carriers. If the grain size is smaller than the mean free path of phonons, the phonons will be predominantly scattered by the grain boundary.

structural disorder seem indispensable in order to enhance zT. Assuming that the mean free paths of charge carriers and phonons are separated in length scales, by preparing chain-oriented polymer fibers (Figure 1b) whose chain lengths are shorter than the mean free path of phonons but longer than that of charge carriers, thermal transport can be significantly suppressed due to the boundary scattering effect of phonons, while charge transport properties are not degraded (Figure 1c).

In this work, inspired by the state-of-the-art experimental progresses, we systematically investigate these hypotheses using rationally designed chain-oriented PEDOT fibers in which both chain length and structural disorder of backbone span a certain range (Table S1, Supporting Information), to examine different strategies on engineering thermal transport in PEDOT for enhanced TE efficiency. A multiscale theoretical approach combining nonequilibrium molecular dynamics (NEMD) simulations and first-principles calculations is employed. We demonstrate that the "ideal" crystalline PEDOT manifests outstanding heat conduction in the polymer backbone direction, yet poor in the interchain direction. The intrachain zT of "ideal" crystalline PEDOT is therefore very poor in spite of its excellent power factor. By tuning the chain length and the crystallinity of chain-oriented PEDOT fibers, a dramatic decrease of the axial thermal conductivity has been observed, from 41.7 W m^{-1} K^{-1} in "ideal" crystalline PEDOT to 0.97 W m^{-1} K^{-1} in rationally designed polymer fibers with the crystallinity of 0.49 and relative molecular weight of 5600. The zT at 298 K has been enhanced to 0.48, which is around 20 times higher than that in the crystalline polymers.

2. Results and Discussion

2.1. "Ideal" Crystalline PEDOT

We first derive the lattice thermal conductivity of "ideal" single crystalline PEDOT, in either pristine or doped form. Both intra- and interchain interactions in PEDOT are characterized by the general Amber force field (GAFF), whose validity has been confirmed by comparing calculated mass density (Table S2, Supporting Information), typical structural parameters (Table S3, Supporting Information), glass transition temperature (Figure S4a, Supporting Information), volumetric thermal expansion coefficient (Figure S4b, Supporting Information), featured vibrational frequencies (Figures S5 and S6 and Table S4, Supporting Information), and heat capacity of PEDOT (Table S5, Supporting Information), with available experimental data and density functional theory (DFT) calculations. The NEMD simulation based on appropriate force fields has been demonstrated as a reliable approach to calculate the lattice thermal conductivity of organic materials,[14] see the Experimental Section for details. By exploiting the velocity-exchange algorithm,[15] a heat flow is generated across the system. After the steady state and local thermal equilibrium

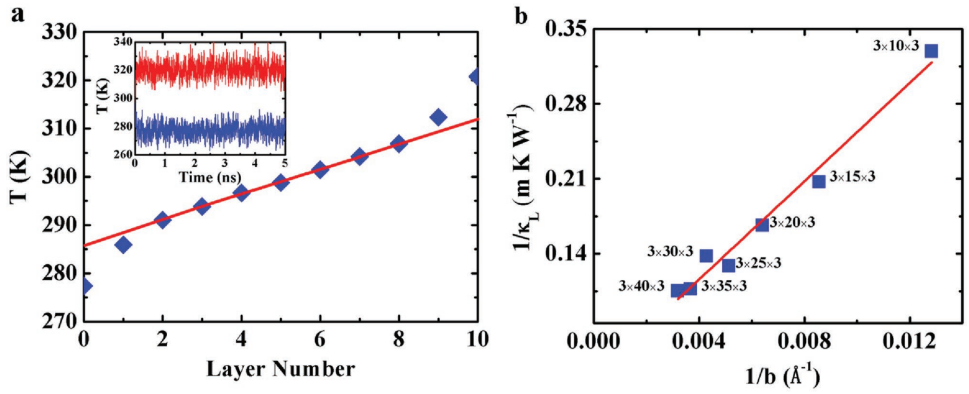

Figure 2. a) Temperature profile obtained from the NEMD simulations at 298 K. The time average of the instantaneous temperature is taken over the final 3 ns of the simulation after the steady state has been established. The solid red line represents a linear fit of the data points. The inset shows the temperature evolution with time for the heat sink (the blue curve) and heat source (the red curve). b) Eliminating the finite-size effect by extrapolation to derive the lattice thermal conductivity of true bulk materials. Inverse of the lattice thermal conductivity, κ_{MD}^{-1} is shown as a function of inverse of the simulation box length, L_{box}^{-1} in the chain direction at 298 K. The solid red line represents a linear fit of the data points. The sizes of supercells in the number of primitive cells are also labeled in the figure.

have been established, a temperature distribution in the system is measured. The lattice thermal conductivity is derived from the heat current and the temperature gradient via Fourier's law, $J_Q = -\kappa_L \nabla T$. The temperature distribution across the system is linear except in the region near the heat sink and heat source (**Figure 2**a) because the unphysical exchange of atomic velocities and the physical heat flow in that region are not balanced. Extrapolation of lattice thermal conductivities at a series of simulation box lengths, see the Experimental Section, has been performed to derive the true bulk lattice thermal conductivity and the phonon mean free path (Figure 2b and Figure S7, Supporting Information).

The "ideal" crystalline PEDOT, either pristine or doped PEDOT:Tos, exhibits the lattice thermal conductivity of 41.7 or 61.2 W m^{-1} K^{-1} in the backbone direction and 0.33 or 0.14 W m^{-1} K^{-1} in the stacking direction (**Table 1**). Doping has little effect on the in-plane thermal transport properties since Tos is intercalated between PEDOT lamellas. The highly anisotropic lattice thermal conductivity has also been observed in highly oriented PE fibers,[16] which is ≈180-fold between intra- and interchain directions and very close to our prediction here for PEDOT. We attribute this anisotropy to the distinct bonding nature in two directions, i.e., strong covalent bonds in the polymer chain direction *versus* weak van der Waals interactions in the stacking direction. Such a high anisotropy is unique to chain-oriented conducting polymers, which makes them distinguishable from small-molecule based organic semiconducting materials. We have surveyed the experimental data available in the literature, which show that lattice thermal conductivities of chain-aligned polymeric materials usually fall in the range of 10–100 W m^{-1} K^{-1} in the chain direction, and those in the perpendicular directions fall in the range of 0.1–1 W m^{-1} K^{-1}. The lattice thermal conductivities of amorphous polymers dictated by weak van der Waals interactions also fall within 0.1–1 W m^{-1} K^{-1} (**Figure 3**a). For example, the total thermal conductivity of amorphous PEDOT:Tos and PEDOT:PSS thin-films was reported to be 0.37[8] and 0.42 W m^{-1} K^{-1},[6] respectively. Moreover, by engineered interchain interactions via hydrogen bonded network, a high lattice thermal conductivity over 1.5 W m^{-1} K^{-1} has been observed in amorphous polymer blends films of poly(*N*-acryloyl piperidine) (PAP) and poly(acrylic acid) (PAA).[17]

According to the kinetic theory of gas for heat conduction, $\kappa_L = c_V v^2 \tau$, the lattice thermal conductivity is proportional to the specific heat capacity (c_V), the phonon group velocity (v), and the phonon relaxation time (τ) arising from phonon scatterings. The phonon group velocity is related to the elastic constant (E) and the mass density (ρ) by $v = \sqrt{E/\rho}$. The phonon relaxation time $\tau = l/v$ is derived from the phonon mean free path (l). Both the elastic constant and the phonon relaxation time show distinct anisotropy in pristine PEDOT and doped PEDOT:Tos crystals. The elastic constants are 190 × 10^9 (232 × 10^9) and

Table 1. Summary of thermal and electrical transport properties for "ideal" crystalline PEDOT. Elastic constant E (in 10^9 J m^{-3}), mass density ρ (in g cm^{-3}), phonon group velocity v (in 10^3 m s^{-1}), phonon and hole mean free paths l_{phonon} and l_{hole} (in Å), phonon relaxation time τ (in ps), heat capacity per volume at constant volume c_V (in J cm^{-3} K^{-1}), and lattice thermal conductivity, κ_L (in W m^{-1} K^{-1}) for pristine PEDOT and lightly doped PEDOT:Tos in the b* and c* directions at 298 K.

	Directions	E	ρ	v	l_{phonon}	τ	c_V	κ_L	l_{hole}
Pristine	b*	232	1.68	11.8	479	4.06	1.49	41.7	13.2
	c*	19.0		3.36	25.0	0.74		0.33	4.17
Lightly doped	b*	195	1.45	11.6	1.11×10^3	9.57	1.32	61.2	4.04
	c*	46.3		5.65	17.8	0.32		0.14	1.24

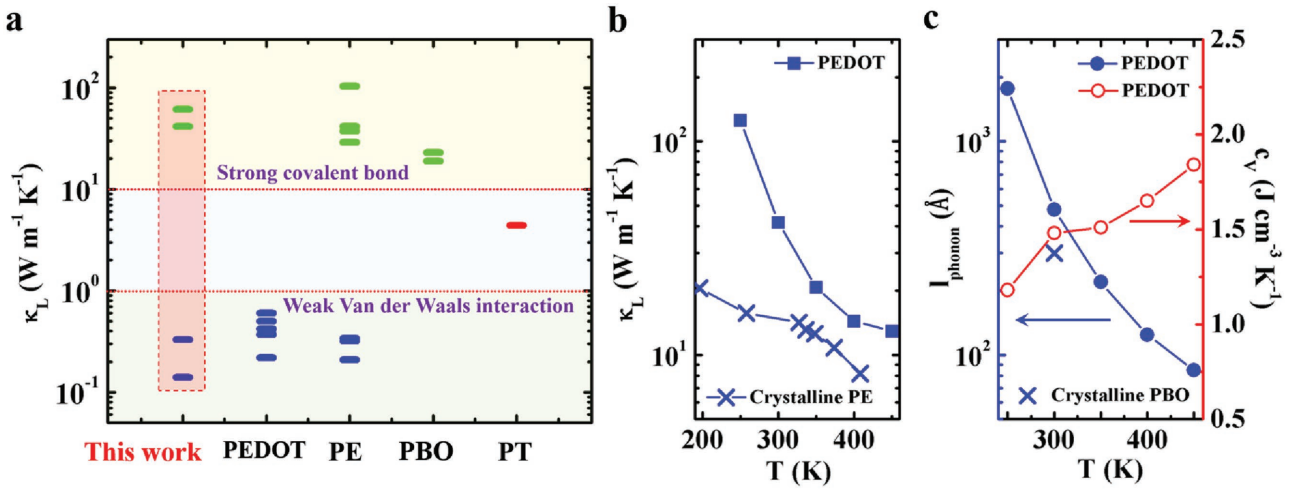

Figure 3. Thermal transport for the "ideal" crystalline PEDOT. a) Lattice thermal conductivities calculated for the pristine PEDOT and lightly doped crystalline PEDOT:Tos at 298 K in the chain (the green bar) and stacking (the blue bar) directions, respectively (in the shaded red box). The measured lattice thermal conductivities of other polymers are displayed for comparison. The related references are listed in the Supporting Information. b) Temperature dependence of the axial lattice thermal conductivity, κ_L. The experimental data of crystalline polymer PE from Ref. [18] are shown for comparison. c) Temperature dependence of the phonon mean free path, l_{phonon} and heat capacity per volume at constant volume, c_V. The experimental l_{phonon} of crystalline PBO fibers from Ref. [18] at room temperature is also displayed.

19×10^9 (46×10^9) J m^{-3}, and the phonon relaxation times are 4 (9) ps and 0.7 (0.3) ps in pristine (doped) PEDOT along the backbone and stacking directions, respectively (Table 1). It has been reported that some typical polymer fibers, such as polybenzobisoxazole (PBO), exhibit high intrinsic axial lattice thermal conductivity (≈20 W m^{-1} K^{-1}), large phonon relaxation time (≈3 ps), and long phonon mean free path (≈300 Å) at the room temperature.[18] The lattice thermal conductivity of crystalline PEDOT decreases rapidly with the increasing temperature (Figure 3b). The measured lattice thermal conductivity of crystalline PE fiber also displays the analogous temperature dependence relationship (Figure 3b).[18] We show that the phonon mean free path decreases dramatically with the increasing temperature, while the heat capacity is insensitive to the temperature (Figure 3c). Because at higher temperatures more phonons are generated, which lead to stronger interactions and substantially reduced phonon mean free path.

The 200-fold anisotropy of lattice thermal conductivities in "ideal" crystalline PEDOT is much higher than the tenfold anisotropy of power factors. As a result, the zT value along the polymer backbone is 0.02 despite of its high power factor, and that in the stacking direction is 0.19 (**Figure 4**). TE conducting polymers are supposed to be electron-crystal and phonon-glass. The above results demonstrate that crystalline conjugated polymers are electron-crystal in the polymer backbone direction and phonon-glass in the stacking and lamellar directions. To take advantage of the high power factor in the direction of polymer backbone, thermal transport in that direction has to be suppressed. In the following, we show that by controlling the chain length of polymers and introducing structural disorders, the lattice thermal conductivity in the backbone direction can be substantially reduced.

To improve TE efficiency of conducting polymers, a challenging task is to reduce the thermal conductivity while not deteriorate the electrical transport properties. The hole mean free path, after considering acoustic phonon and ionized impurity scatterings, is predicted to be 13.2 Å in pristine PEDOT and 4.04 Å in doped PEDOT:Tos, which is more than one order of magnitude smaller than the phonon mean free path, 479 Å in pristine PEDOT and 1000 Å in doped PEDOT:Tos (Table 1). If the polymer chain is longer than the mean free path of charge carriers but shorter than that of phonons, the lattice thermal conductivity will be significantly reduced due to the phonon scattering at boundaries while charge transport will be minimally affected. So engineering the chain length of polymers is one of effective strategies to enhance zT. The estimated

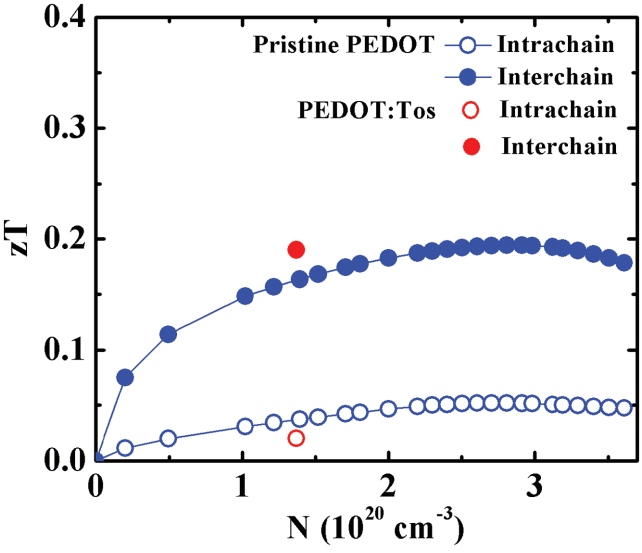

Figure 4. Dimensionless TE figure of merit, zT for the "ideal" crystalline pristine PEDOT and explicit lightly doped PEDOT:Tos in the intrachain and interchain directions as a function of the hole concentration at 298 K.

room-temperature hole mean free paths of crystalline pristine (4.2 Å) and lightly doped PEDOT (1.2 Å) in the π–π stacking direction are consistent with that of naphthalene single crystal (1.5 Å) predicted by Silbey and co-authors.[19] The relative molecular weight (r.m.w.) of polymers usually spans from 10^4 to 10^6 and exhibits a distribution. To suppress thermal transport in the backbone direction, the chain length of PEDOT should be larger than 13.2 Å and smaller than 479 Å, which amounts to 4–124 EDOT units and r.m.w. of 560–17 360. Based on the "ideal" crystalline PEDOT, we designed two polymers, **Polymer 1** and **Polymer 2**, whose chain length is 156 and 391 Å, r.m.w. is 5600 and 14 000, containing 40 and 100 EDOT moieties, respectively. We derived their lattice thermal conductivities, which are 4.84 and 9.84 W m^{-1} K^{-1}, respectively, reduced by nine and four times with respect to the "ideal" crystalline PEDOT due to the size effect. The chain length of these two polymers is much longer than the mean free path of holes, so charge movement in them will be barely affected, and we expect the zT value be enhanced to 0.16 in **Polymer 1** and 0.09 in **Polymer 2**. These results clearly demonstrate that thermal transport in conducting polymers can be effectively suppressed by controlling their degree of polymerization.

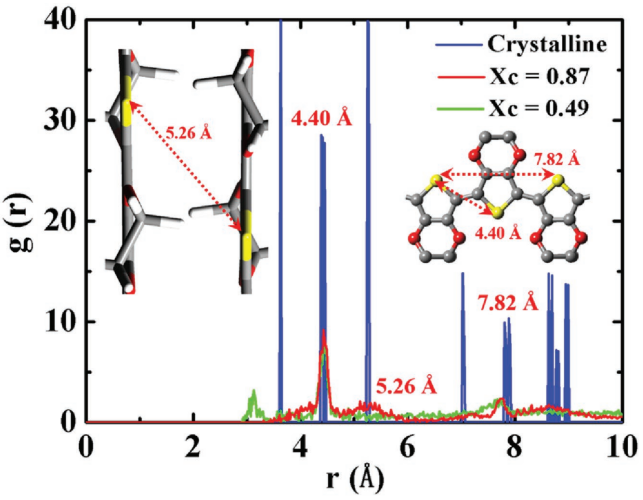

Figure 5. Radial distribution function, $g(r)$ between sulfur atoms for crystalline PEDOT and two fibers with the crystallinity X_c = 0.49 and X_c = 0.87 at 298 K. The r.m.w. of both fibers is 5600. The insets show the structures of PEDOT in the backbone and π–π stacking directions, in which the typical distances between sulfur atoms are labeled.

2.2. Chain-Oriented PEDOT Fibers

In practice, it is difficult to grow crystalline polymers from the solution process, yet chain-oriented polymer fibers with structural disorder are easy to fabricate, in which heat transfer may be further hindered by localized vibrations. We prepared series of chain-oriented fibers with various degrees of structural disorder based on **Polymer 1** and **Polymer 2** by the simulated thermal annealing approach, see the Experimental Section. The structural disorder of polymer fibers is characterized by a physical parameter, the crystallinity, X_c. The volume crystallinity is defined as $X_c = (\rho - \rho_a)/(\rho_c - \rho_a)$, where ρ is the mass density of our samples, ρ_a = 1.00 g cm^{-3},[20] and ρ_c = 1.68 g cm^{-3} based on our DFT calculations, represent mass densities of amorphous and "ideal" crystalline PEDOT, respectively. With the increase of structural disorder, the volume crystallinity decreases from 0.87 to 0.49 for **Polymer 1** and from 0.89 to 0.54 for **Polymer 2**. The structural disorder is also manifested by the radial distribution function (RDF) of sulfur–sulfur distance in the thiophene ring of 3,4-ethylenedioxythiophene (EDOT), which shows broader peaks in chain-oriented fibers than in crystalline PEDOT, except for the one contributed by the nearest-neighbor sulfur atoms (≈4.40 Å) along the polymer backbone (**Figure 5**). The broader distribution indicates the poorer crystallinity.

We derived lattice thermal conductivities of these rationally designed fibers by the same NEMD method. The relationship between the axial lattice thermal conductivity and the sample crystallinity is shown in **Figure 6**a. The lattice thermal conductivity correlated strongly with the crystallinity of polymers. As the crystallinity decreases from 0.87 to 0.49, the lattice thermal conductivity is reduced from 4.88 to 0.97 W m^{-1} K^{-1} in **Polymer 1**, and as the crystallinity decreases from 0.89 to 0.54, the lattice thermal conductivity is reduced from 6.66 to 1.67 W m^{-1} K^{-1} in **Polymer 2**, in contrast to 41.7 W m^{-1} K^{-1} in "ideal" crystalline PEDOT. Moreover, with the crystallinity decreasing, the lattice thermal conductivity in polymers with longer chains drops faster than shorter chains, which indicates that heat propagation in the latter is more seriously hindered by localized vibrations.

The temperature dependence of the lattice thermal conductivity in amorphous PEDOT fibers is different from that in crystalline PEDOT. With the temperature rising, the lattice thermal conductivity of chain-oriented PEDOT fibers increases slightly (Figure 6b), which is typical for amorphous materials, such as amorphous polymer blends films of PAP and PAA (Figure 6b).[17] The mechanisms of thermal transport in amorphous solids are not yet completely understood. Theoretical models, including constant phonon mean free path picture,[21] the minimum thermal conductivity model,[22] Kubo based theory,[23] anharmonic interactions between localized vibrations,[24] and delocalized phonon-like modes,[25] have been proposed to understand the thermal conductivity and temperature relationship. Our simulation results show that the specific heat capacity increases slightly with the increasing temperature from 250 to 450 K (Figure 6c), which gives rise to the slow increment of the lattice thermal conductivity. However, we cannot rule out the possibility that as the temperature increases, the anharmonic interactions between localized vibrations are strengthened, which results in the further increment of lattice thermal conductivity.[24] In addition, as the chain length increases, the lattice thermal conductivity increases obviously, which we attribute to the contribution of delocalized phonon-like modes to heat conduction.[25]

By controlling the chain length and introducing structural disorder, the zT value of **Polymer 1**, X_c of 0.49 and r.m.w. of 5600, is enhanced to 0.48 in the axial direction (**Figure 7**), which is 20 times higher than the "ideal" crystalline PEDOT. Our results highlight that by tailoring the degree of polymerization and crystallization, thermal transport in chain-oriented

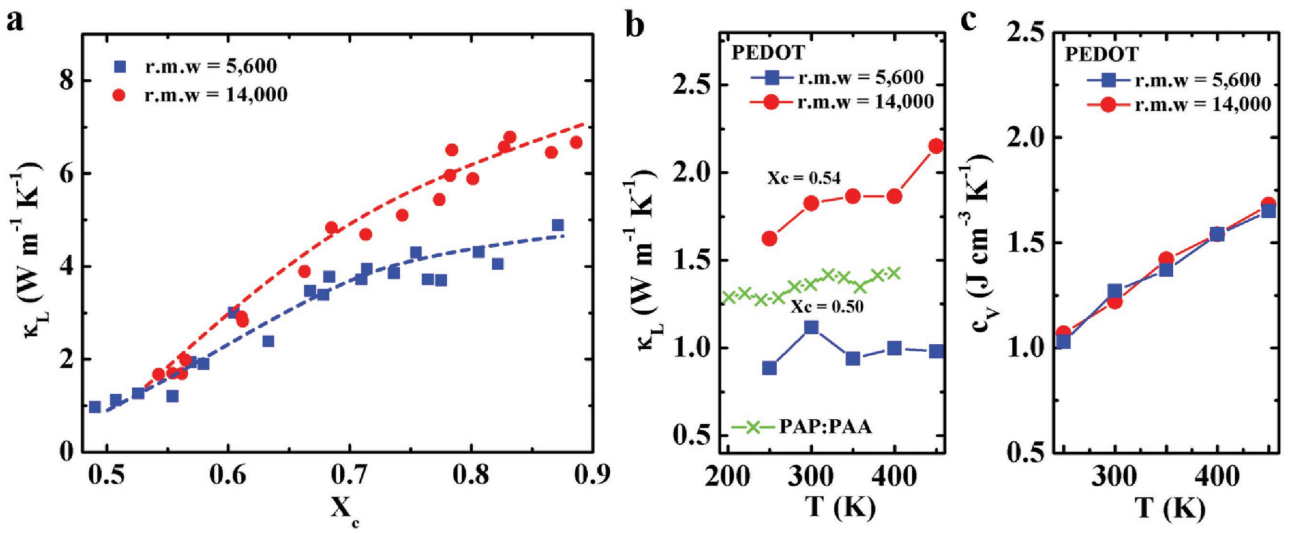

Figure 6. Engineering thermal transport in the chain-oriented PEDOT fibers by controlling the degree of polymerization and the crystallinity. a) Relationship between the axial lattice thermal conductivity, κ_L of chain-oriented PEDOT fibers and the sample crystallinity, X_c at 298 K. The dashed lines are shown to guide the eyes of the trend. b) Temperature dependence of the axial lattice thermal conductivity, κ_L for two chain-oriented amorphous PEDOT fibers. The experimental data of amorphous polymer blend films of poly(*N*-acryloyl piperidine) (PAP) and poly(acrylic acid) (PAA) from Ref. [17] are shown for comparison. c) Temperature dependence of heat capacity per volume at constant volume, c_V of the same fibers as in (b).

polymeric fibers can be substantially suppressed. These seminal studies on engineering thermal transport in conducting polymers open up alternative strategies to doping optimization for achieving high TE efficiency.

3. Conclusions

In summary, we have shown that crystalline PEDOT is an excellent heat conductor in the direction of polymer backbone, but it is phonon-glass in the interchain directions due to its anisotropic chemical bonding nature, covalent *versus* van der Waals bondings. The TE efficiency of crystalline PEDOT is thus very poor in the chain direction despite of its electron-crystal nature. We highlight effective strategies to engineer thermal transport along the polymer backbone for achieving high TE figure of merit, based on the separated length scales of charge and phonon transport. By the rational design and tailoring the chain length and crystallinity of chain-oriented PEDOT fibers, a significant decrease of the lattice thermal conductivity from 41.7 to 0.97 W m^{-1} K^{-1}, and an impressive increase of zT from 0.02 to 0.48 have been attained. The degree of polymerization and crystallization are two important factors governing thermal transport in polymers. Both of them can be controlled during fabrication and characterized experimentally. We believe that the strategies suggested here for engineering thermal transport are robust and applicable to other TE conducting polymers.

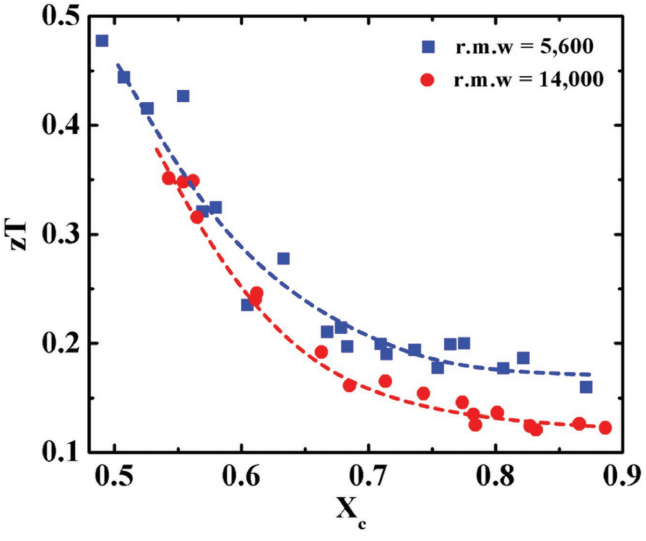

Figure 7. Engineering dimensionless TE figure of merit in the chain-oriented PEDOT fibers by controlling the degree of polymerization and the crystallinity. The dependence of TE figure of merit, zT on the sample crystallinity, X_c for the lightly doped PEDOT:Tos at 298 K. The dashed lines are shown to guide the eyes of the trend.

4. Experimental Section

Model Setup: "Ideal" crystalline models of pristine PEDOT and lightly doped PEDOT:Tos with infinitely long chain length were taken from Ref. [26] and the previous work.[10] It was started from the crystal structure of "ideal" pristine PEDOT with 18 chains in the cell and built model structures for Polymer 1 and Polymer 2 by retaining 40 and 100 EDOT moieties respectively in each chain (Table S1, Supporting Information). Based on these two crystalline models of different chain lengths, chain-oriented polymer fibers were generated by the simulated thermal annealing approach as follows. The initial crystalline structures were first heated to and equilibrated at temperatures between 500 and 1800 K for 500 ps in the canonical (NVT) ensemble with Nosé–Hoover thermostat and then cooled down to 298 K at a rate of 0.1–5 K ps^{-1} under the isotropic control of pressure at 1 atm. The system was then equilibrated in the NVT ensemble for 500 ps and subsequently isothermal-isobaric (NPT) ensembles for 500 ps with

Nosé–Hoover thermostat and barostat at the temperature of 298 K and the pressure of 1 atm. The GAFF with anharmonic interactions included was used to describe the bonded and nonbonded interactions of PEDOT and Tos.[27] The atomic partial charges were derived by the restrained electrostatic potential fitting method.[28] The real-space cutoff radius for Coulombic and Lennard-Jones interactions was set to be 10 Å. The long-range Coulombic and $1/r^6$ dispersion interactions were computed by the particle–particle particle–mesh (pppm) method.[29] The velocity Verlet algorithm was used to update the positions and velocities of atoms. The time step for integration of the equation of motion was set to be 1 fs. The simulations were performed with the large-scale atomic/molecular massively parallel simulator package.[30]

Lattice Thermal Conductivity Calculation: The NEMD simulations were applied to mimic the thermal transport process.[31] In this approach, a heat flux JQ across the system was generated, and the resulting temperature gradient ∇T was measured after the system had established a steady state. The lattice thermal conductivity κ_L can be extracted according to the Fourier's law, $J_Q = -\kappa_L \nabla T$. Herein the Müller–Plathe velocity-exchange algorithm was used to generate the heat flux in the system.[15] The velocity swapping was conducted every 200 steps. Over time, this introduced a temperature gradient in the system. The total NEMD simulations lasted for 5 ns. To correct the finite-size effect, the simulations were performed at several box lengths, and the thermal conductivity data were extrapolated to derive the lattice thermal conductivity of true bulk crystal according to the formula

$$\frac{1}{\kappa_{MD}} = \frac{3}{c_V \nu^2} \tau_{MD}^{-1} = \frac{3}{c_V \nu^2} \left(\frac{1}{\tau_{bulk}} + \frac{2\nu}{L_{box}} \right) \equiv A + \frac{B}{L_{box}} \quad (1)$$

where κ_{MD} and L_{box} are the lattice thermal conductivity obtained from the NEMD simulations and the corresponding box length (Figure 2b and Figure S7, Supporting Information).[32] The phonon mean free paths, l_{bulk} were obtained according to Equation (1) via the relation $l_{bulk} = \nu \tau_{bulk} = B/2A$, where τ_{bulk} is the phonon relaxation time. The more details of methods were provided in the Supporting Information.

Supporting Information

Supporting Information is available from the Wiley Online Library or from the author.

Acknowledgements

This work was supported by the National Natural Science Foundation of China (Grant Nos. 21673123, 21290190, 21290191, and 91333202) and the Ministry of Science and Technology of China (Grant Nos. 2015CB655002 and 2013CB933503). Computational resources were provided by the Tsinghua Supercomputing Center.

Conflict of Interest

The authors declare no conflict of interest.

Keywords

molecular dynamics simulations, poly(3,4-ethylenedioxythiophene) (PEDOT), thermal transport, thermoelectrics

Received: May 27, 2017
Revised: July 14, 2017
Published online: August 29, 2017

[1] a) O. Bubnova, X. Crispin, *Energy Environ. Sci.* **2012**, *5*, 9345; b) M. He, F. Qiu, Z. Lin, *Energy Environ. Sci.* **2013**, *6*, 1352; c) Q. Zhang, Y. Sun, W. Xu, D. Zhu, *Adv. Mater.* **2014**, *26*, 6829; d) B. T. McGrail, A. Sehirlioglu, E. Pentzer, *Angew. Chem. Int. Ed.* **2015**, *54*, 1710; e) Y. Chen, Y. Zhao, Z. Liang, *Energy Environ. Sci.* **2015**, *8*, 401; f) B. Russ, A. Glaudell, J. J. Urban, M. L. Chabinyc, R. A. Segalman, *Nat. Rev. Mater.* **2016**, *1*, 16050.

[2] a) F. J. DiSalvo, *Science* **1999**, *285*, 703; b) L. E. Bell, *Science* **2008**, *321*, 1457.

[3] a) G. A. Slack, in *CRC Handbook of Thermoelectrics*, CRC Press, Boca Raton **1995**; b) M. Beekman, D. T. Morelli, G. S. Nolas, *Nat. Mater.* **2015**, *14*, 1182.

[4] a) G. J. Snyder, E. S. Toberer, *Nat. Mater.* **2008**, *7*, 105; b) J. P. Heremans, V. Jovovic, E. S. Toberer, A. Saramat, K. Kurosaki, A. Charoenphakdee, S. Yamanaka, G. J. Snyder, *Science* **2008**, *321*, 554; c) A. I. Hochbaum, R. K. Chen, R. D. Delgado, W. J. Liang, E. C. Garnett, M. Najarian, A. Majumdar, P. D. Yang, *Nature* **2008**, *451*, 163; d) Y. Z. Pei, X. Y. Shi, A. LaLonde, H. Wang, L. D. Chen, G. J. Snyder, *Nature* **2011**, *473*, 66; e) K. Biswas, J. He, I. D. Blum, C.-I. Wu, T. P. Hogan, D. N. Seidman, V. P. Dravid, M. G. Kanatzidis, *Nature* **2012**, *489*, 414; f) J. P. Heremans, M. S. Dresselhaus, L. E. Bell, D. T. Morelli, *Nat. Nanotechnol.* **2013**, *8*, 471; g) L. D. Zhao, S. H. Lo, Y. S. Zhang, H. Sun, G. J. Tan, C. Uher, C. Wolverton, V. P. Dravid, M. G. Kanatzidis, *Nature* **2014**, *508*, 373; h) L.-D. Zhao, G. Tan, S. Hao, J. He, Y. Pei, H. Chi, H. Wang, S. Gong, H. Xu, V. P. Dravid, C. Uher, G. J. Snyder, C. Wolverton, M. G. Kanatzidis, *Science* **2016**, *351*, 141.

[5] a) O. Bubnova, M. Berggren, X. Crispin, *J. Am. Chem. Soc.* **2012**, *134*, 16456; b) Z. U. Khan, J. Edberg, M. M. Hamedi, R. Gabrielsson, H. Granberg, L. Wågberg, I. Engquist, M. Berggren, X. Crispin, *Adv. Mater.* **2016**, *28*, 4556.

[6] G. H. Kim, L. Shao, K. Zhang, K. P. Pipe, *Nat. Mater.* **2013**, *12*, 719.

[7] F. X. Jiang, J. K. Xu, B. Y. Lu, Y. Xie, R. J. Huang, L. F. Li, *Chin. Phys. Lett.* **2008**, *25*, 2202.

[8] O. Bubnova, Z. U. Khan, A. Malti, S. Braun, M. Fahlman, M. Berggren, X. Crispin, *Nat. Mater.* **2011**, *10*, 429.

[9] T. Park, C. Park, B. Kim, H. Shin, E. Kim, *Energy Environ. Sci.* **2013**, *6*, 788.

[10] W. Shi, T. Zhao, J. Xi, D. Wang, Z. Shuai, *J. Am. Chem. Soc.* **2015**, *137*, 12929.

[11] a) H. R. Tseng, H. Phan, C. Luo, M. Wang, L. A. Perez, S. N. Patel, L. Ying, E. J. Kramer, T. Q. Nguyen, G. C. Bazan, A. J. Heeger, *Adv. Mater.* **2014**, *26*, 2993; b) C. Luo, A. K. K. Kyaw, L. A. Perez, S. Patel, M. Wang, B. Grimm, G. C. Bazan, E. J. Kramer, A. J. Heeger, *Nano Lett.* **2014**, *14*, 2764.

[12] O. Bubnova, Z. U. Khan, H. Wang, S. Braun, D. R. Evans, M. Fabretto, P. Hojati-Talemi, D. Dagnelund, J.-B. Arlin, Y. H. Geerts, S. Desbief, D. W. Breiby, J. W. Andreasen, R. Lazzaroni, W. M. Chen, I. Zozoulenko, M. Fahlman, P. J. Murphy, M. Berggren, X. Crispin, *Nat. Mater.* **2014**, *13*, 190.

[13] S. Shen, A. Henry, J. Tong, R. Zheng, G. Chen, *Nat. Nanotechnol.* **2010**, *5*, 251.

[14] a) J. Chen, D. Wang, Z. Shuai, *J. Chem. Theory Comput.* **2012**, *8*, 3338; b) W. Shi, J. Chen, J. Xi, D. Wang, Z. Shuai, *Chem. Mater.* **2014**, *26*, 2669.

[15] F. Müller-Plathe, *J. Chem. Phys.* **1997**, *106*, 6082.

[16] D. B. Mergenthaler, M. Pietralla, S. Roy, H. G. Kilian, *Macromolecules* **1992**, *25*, 3500.

[17] G.-H. Kim, D. Lee, A. Shanker, L. Shao, M. S. Kwon, D. Gidley, J. Kim, K. P. Pipe, *Nat. Mater.* **2015**, *14*, 295.

[18] X. Wang, V. Ho, R. A. Segalman, D. G. Cahill, *Macromolecules* **2013**, *46*, 4937.

[19] Y. C. Cheng, R. J. Silbey, D. A. da Silva, J. P. Calbert, J. Cornil, J. L. Bredas, *J. Chem. Phys.* **2003**, *118*, 3764.

[20] A. Elschner, S. Kirchmeyer, W. Lövenich, U. Merker, K. Reuter, *PEDOT: Principles and Applications of an Intrinsically Conductive Polymer*, CRC Press, Boca Raton **2011**.
[21] C. Kittel, *Phys. Rev.* **1949**, *75*, 972.
[22] W.-P. Hsieh, M. D. Losego, P. V. Braun, S. Shenogin, P. Keblinski, D. G. Cahill, *Phys. Rev. B* **2011**, *83*, 174205.
[23] P. B. Allen, J. L. Feldman, *Phys. Rev. Lett.* **1989**, *62*, 645.
[24] S. Shenogin, A. Bodapati, P. Keblinski, A. J. H. McGaughey, *J. Appl. Phys.* **2009**, *105*, 034906.
[25] K. T. Regner, D. P. Sellan, Z. Su, C. H. Amon, A. J. H. McGaughey, J. A. Malen, *Nat. Commun.* **2013**, *4*, 1640.
[26] E.-G. Kim, J.-L. Brédas, *J. Am. Chem. Soc.* **2008**, *130*, 16880.
[27] J. Wang, R. M. Wolf, J. W. Caldwell, P. A. Kollman, D. A. Case, *J. Comput. Chem.* **2004**, *25*, 1157.
[28] W. D. Cornell, P. Cieplak, C. I. Bayly, P. A. Kollmann, *J. Am. Chem. Soc.* **1993**, *115*, 9620.
[29] R. W. Hockney, J. W. Eastwood, *Computer Simulation Using Particles*, Taylor & Francis Inc., Oxfordshire **1989**.
[30] S. Plimpton, *J. Comput. Phys.* **1995**, *117*, 1.
[31] D. Wang, L. Tang, M. Long, Z. Shuai, *J. Phys. Chem. C* **2011**, *115*, 5940.
[32] H. Jiang, E. M. Myshakin, K. D. Jordan, R. P. Warzinski, *J. Phys. Chem. B* **2008**, *112*, 10207.